JOURNAL OF NANO- AND ELECTRONIC PHYSICS
Vol. **7** No 3, 03009(6pp) (2015)

ЖУРНАЛ НАНО- ТА ЕЛЕКТРОННОЇ ФІЗИКИ
Том **7** № 3, 03009(6cc) (2015)

Influence of the Calcination Temperature on the Combustion Synthesized Perovskite $LaMnO_3$ Compound

A.R. Shelke, N.G. Deshpande*

Department of Physics, Shivaji University, Kolhapur-416004 (M.S.), India

(Received 30 April 2015; revised manuscript received 15 October 2015; published online 20 October 2015)

A simple combustion method based on principles of propellent chemistry in which Polyvinyl alcohol (PVA) as fuel and nitrates as oxidizer were used for synthesizing the perovskite like $LaMnO_3$ powders. The oxidizer to fuel ratio was maintained at 5 : 1. The darkish black powder obtained was calcined at 800 °C and 1000 °C for 5 hour. The combustion and thermal decomposition of the precursor were investigated using the TG-DTA and Fourier Transform Infra-Red (FT-IR) techniques. The X-ray diffraction (XRD) pattern of all three samples i.e., un-heated $LaMnO_3$ powder (LMO-UH), calcined at 800 °C (LMO-800) and at 1000 °C (LMO-1000) were carried out. The single phase orthorhombic crystal structure was revealed to crystallize at LMO-800 and LMO-1000 with elevation in the crystalline size. A small impurity peak at 28.7° was seen of Mn_3O_4 for LMO-UH, which vanished after calcining it. The strong absorption in FT-IR spectra found at around 615 cm^{-1} was due to the formation of metal-oxygen (M-O) bond. Moreover a small shift in this M-O bond with increase in calcination temperature suggested the strained $LaMnO_3$ compound. Elemental analysis using the energy dispersive X-ray fluorescence spectrometer (EDXRF) indicated the presence of La and Mn with increase in the Mn contents after calcinations. The oxygen, nitrogen and hydrogen content in the sample were determined from the ONH analysis indicating a decrease in the oxygen content for LMO-800. Well defined porous-foam like morphology of the sample was achieved from scanning electron microscopic (SEM) study, which become compact with calcination process. Magnetic properties were found to transform from the ferromagnetic-to-paramagnetic phase for LMO-UH sample, while reduction in magnetization values and coercivity at low temperatures was obtained for LMO-800 and LMO-1000 samples.

Keywords: $LaMnO_3$, Structural property, FTIR, Compositional property, and Magnetic property.

PACS numbers: 61.05.cp, 68.37.Hk, 71.30. + h, 75.47.Gk, 75.20. – g

1. INTRODUCTION

A strong interplay between the structural distortion, transport and magnetic properties of the perovskite manganite particularly, $LaMnO_3$ depict interesting physical properties such as antiferromagnetic-insulator, ferromagnetic-metal as well as charge-ordering phenomenon [1-4]. In addition to antiferromagnetism, the parent compound $LaMnO_3$ probably shows some novel phenomenon such as spin-canting, spin-glass, ferromagnetic-insulator with the substitution of cations at different sites [5-6]. The corresponding properties arise depending on the off-stoichiometric cation substitution on the lanthanum or manganese site [7]. Such a system results into decisive magnetic properties of the $LaMnO_3$ giving the colossal magnetoresistance (CMR) effect and other novel magnetic phenomenon. Recently, researcher tried to develop its structural as well as physical properties by substituting different types of divalent or tetravalent cations to behave like the hole or electron-doped system, respectively [8]. The cation substitution effect into the $LaMnO_3$ matrix, enhances the magnetic properties by coupling mechanism and novel Jahn-Teller distortion in MnO_6 octahedron [9-11]. However, the Lanthanium and / or oxygen non-stoichiometry in the $LaMnO_3$ compound produces the vacancies. This results into either $La_{1-x}MnO_3$ or $LaMnO_{3\pm\delta}$ system that exhibits properties of self-doping effect and produces the mixed valence state of the Mn viz. Mn^{3+} and Mn^{4+} to fulfill the charge neutrality [12]. This establishment of the mixed valence state in the $LaMnO_3$ compound enhances the coexistence of ferromagnetic double exchange and antiferromagnetic super-exchange interactions.

Importantly, all the structural and physical properties of the $LaMnO_3$ compound depend on the method used for synthesis [13-15]. Available reports suggest that there are several physical as well as chemical methods for the synthesis of the $LaMnO_3$ compound both in powder / pellet and thin film forms [13-18]. It is found that two phases viz. orthorhombic and rhombohedral can be synthesized at room / elevated temperatures by using both the aforementioned methods. Significantly, these two phases compete with each other depending on the oxygen off-stoichiometry, which forms the deficiency in the crystal structure. As a result the system behaves as self-doped system and exhibit the interesting CMR effect as discussed earlier [19, 20]. The oxygen off-stoichiometric self-doping of the $LaMnO_3$ can possibly lead in the distortion of the MnO_6 octahedron due to the Jahn-Teller effect that arises during the formation of the mixed valence state of the Mn^{3+} and Mn^{4+}. Orgiani et al. [21] showed that the mixed valence Mn^{3+}/Mn^{4+} population is obtained by self doping of Mn into the La site and resultant La^{3+}/Mn^{2+} induces the required distortions in the MnO_6 cage. The produced distortion in the MnO_6 octahedron favours the hooping of the charge transportation through the corresponding site of $LaMnO_3$ viz. La^{3+}/Mn^{2+} rather than traditional Mn^{3+}/Mn^{4+} path and this is the key point to the for-

* nicedeshpande@gmail.com

mation of the ferromagnetic state in the $LaMnO_3$ compound [21, 22]. Conclusively, the deficiency in the metal side (La or Mn) can create Mn^{4+} (holes) and in order to neutralize this hole, the $LaMnO_3$ system should establish self-doping phenomenon. The neutralization of the hole by self-doping can cause the delocalisation of the electron in the vicinity of the perovskite structure of $LaMnO_3$. This delocalisation forces the spins to align ferromagnetically in a-b plane. Such a magnetic phase transition in the $LaMnO_3$ compound is found recently; eventhough the magnetic structure has been known from anciently [23, 24]. The Jahn-Teller distortion in the system is reduced by giving the heat treatment at comparatively higher temperature, but interestingly structure remains in the orthorhombic phase, which crystallizes in the same *pbnm* space group [23]. This is because the oxygen does not allow to occupy the interstices of the perovskite $LaMnO_3$, hence, it produces the cation vacancies. The corresponding lattice of the structure easily adopts the excess oxygen from the stoichiometric phase of the $LaMnO_3$ [25, 26]. Above mentioned reports suggest that instead of doping $LaMnO_3$ externally to achieve enhanced magneto-transport properties; one can achieve similar properties by self-doping of $LaMnO_3$. Such a self-doping mechanism can be achieved by simply calcining the $LaMnO_3$ at different temperatures, varying the La / Mn ratios and/or by oxygenating the $LaMnO_3$ compound.

Therefore, the present work is an attempt to study this temperature-dependent transformation of $LaMnO_3$ powder samples. It is a try to visualize the correlation of the crystalline structure and the magnetic property of the $LaMnO_3$ synthesized by the simple chemical combustion method. Moreover, the influence of the calcinations temperature on the structural and magnetic properties of the perovskite $LaMnO_3$ powder have been studied and discussed herein.

2. COMBUSTION SYNTHESIS AND THERMAL DECOMPOSITION ANALYSIS

Chemical combustion synthesis is a simple exothermic chemical reaction process that occurs between the fuel and the oxidant according to the principles of the propellant chemistry. Here in the present synthesis we have used poly vinyl alcohol (PVA), which is a synthetic polymer that acts as a fuel. This is for the reason that it gets easily oxidized by nitrate ions. There is a general assumption that PVA conducts the redox reaction with nitrate to ignite the combustion reaction, so that the nitrates partially decompose after heating. The decomposition of the nitrates releases the nitrogen, carbon monoxide, and water molecule in the gaseous form. Therefore, we took 4.33 gm of $La(NO_3)_3$, 1.8 gm of $Mn(NO_3)_3$ and 2.07 gm of PVA as source materials to prepare 0.1 M solution for the combustion reaction process. Importantly, an equivalent weight ratio of 5:1 is maintained between oxidant and the fuel. Thermal decomposition of the above synthesized material have been studied by measuring the TG-DTA of $LaMnO_3$, which is shown in the Fig. 1. It is seen from Fig. 1 that the endothermic peak appears at ~ 70 °C with respective weight loss of 18 %. This endothermic peak is appeared due to the vaporisation of surface absorbed volatile aqueous liquid like water in the composite fabric. Moreover, the extreme reduction in weight loss was occurred at 490 °C, which designates the coupling of DTA peaks with TGA weight loss. This indicates that the autocombustion reaction step occurs at 490 °C due to the decomposition of the reactant viz. nitrate, acetate, PVA etc. by showing the exothermic peak at the corresponding temperature. The total weight loss during the decomposition is up to 56.85 %. At this stage the oxidation of main chain in the PVA is accompanied by the reaction. TG-DTA curves are stable above 700 °C indicating that all the aqueous liquids, organic compounds as well as all nitrate and acetate in the composite fabric were completely volatized and porous inorganic compound of $LaMnO_3$ could be obtained above 700 °C. This obtained information was useful for further calcining our synthesized material at 800 °C and 1000 °C and hence to study the influence of the calcining temperature on the material properties.

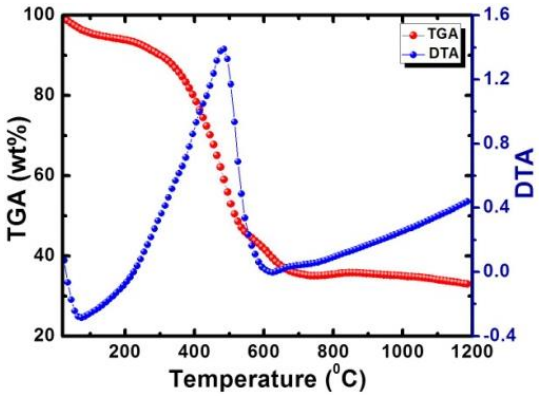

Fig. 1 – Plot of TG-DTA for thermal decomposition analysis of LMO sample

The structural studies were carried out using X-Ray diffractometer model D3-phaser. The chemical composition of the elements present in the material was studied using Energy dispersive X-ray fluorescence (EDXRF) model ARL™ QUANT'X EDXRF Spectrometer and with ONH analyzer. Surface morphology was studied using scanning electron microscopy (SEM) model JEOL JSM-6360. Magnetic measurements were done using SQUID from Quantum design model MPMS3.

3. RESULTS AND DISCUSSION

X-ray diffraction (XRD) spectra are displayed in the Fig. 2 (a) that was carried out for the structural phase determination. The complete phase transformations with different heat treatments are clearly depicted from the obtained XRD data. LMO-UH showed $LaMnO_3$ sample peaks along with some impurity peaks at $2\theta = 28.7°$. This peak originates from the un-reacted Mn_3O_4. The orthorhombic structure having single phase was obtained from the JCPDS data card no. 00-033-0713 for LMO-800 sample. In addition to this a broad hump around $2\theta \sim 28°$ with low angle shift in the peak positions was obtained for LMO-1000 sample. The average crystalline size of LMO-800 was calculated to be 11 nm; while, for the LMO-UH and LMO-1000, it is 7 nm and 13 nm, respectively. The modification of crystalline state

in the case of $LaMnO_3$ calcined at 800 °C is due to the reduction of excess oxygen in the interstitial sites accompanied with formation of the Mn^{3+} state [27]. This elevation in the crystalline size of LMO-800 may result into the reduction of the ferromagnetic-metallic behaviour of $LaMnO_3$. The result of rietveld refinement fitting is displayed in the Fig. 2 (b), especially, done for LMO-800 sample. The rietvield refinement confirms the single phase orthorhombic structure fitted in the *pbnm* space group with no detectable secondary phase when the sample is calcined at 800 °C. The discrepancy factors obtained from the rietvield refinement were; $R_p = 45.5$ %, $R_{wp} = 36.0$ %, $R_{exp.} = 27.15$ % and $\chi^2 = 1.75$. The lattice parameters obtained from the rietvield fitting are $a = 5.5461$ Å, $b = 5.5990$ Å, $c = 7.8152$ Å and $\alpha = \beta = \gamma = 90°$. Apart from this a small distortion [see Fig. 2 (c)] in the structural model of the $LaMnO_3$ in MnO_6 cage appeared due to the localized stress field during the crystallization process. The resultant physical properties viz. magnetization, transportation of the charge carriers are strongly affected on this structural distortion. As prepared sample shows the small Mn_3O_4 impurities phase in addition to the orthorhombic $LaMnO_3$. Further calcinations of the $LaMnO_3$ powder at 1000 °C shows the slight shift at lower angle due to the residual stress field produced at higher temperature, which also produce the defect in the material and may give a hump in the background signal [28]. So, the more crystalline nature of the compound calcined at 800 °C shows the occurrence of complete combustion reaction [29].

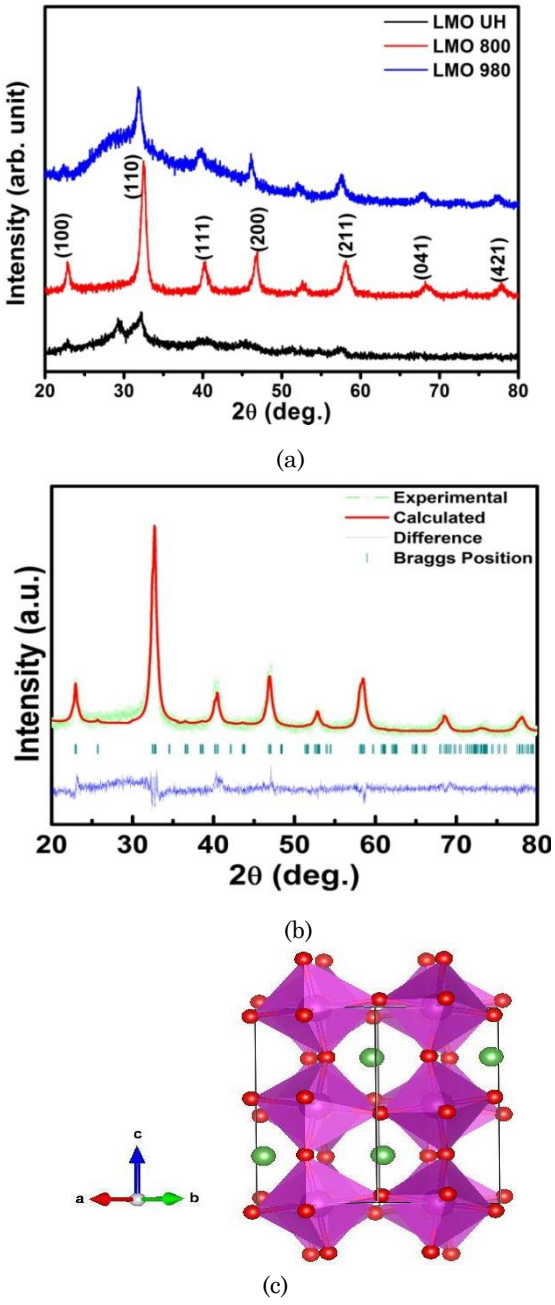

Fig. 2 – (a) XRD of LMO-UH, LMO-800 and LMO-1000 samples. (b) Reitveled fitting and crystal structure of LMO-800 (c) Structural Model of LMO-800 showing distortions in MnO_6 octahedra

Fig. 3 (a) illustrates FT-IR spectra of $LaMnO_3$ perovskite compound. For LMO-UH sample, one can see a broad peak originating around 585 cm^{-1}. This peak is found to be shifted towards higher frequency i.e., 615 cm^{-1} when calcined at 800 °C and 1000 °C for samples LMO-800 and LMO 1000, respectively. The obtained peak at 615 cm^{-1} is reported to be of the stretching mode, which involves the internal motion of a change in Mn-O-Mn bond length [30].

This is an indication that the metal-oxygen (M-O) bonds are subsequently organized into a MnO_6 octahedral structure, representing the formation of crystalline LMO powder containing the perovskite structure

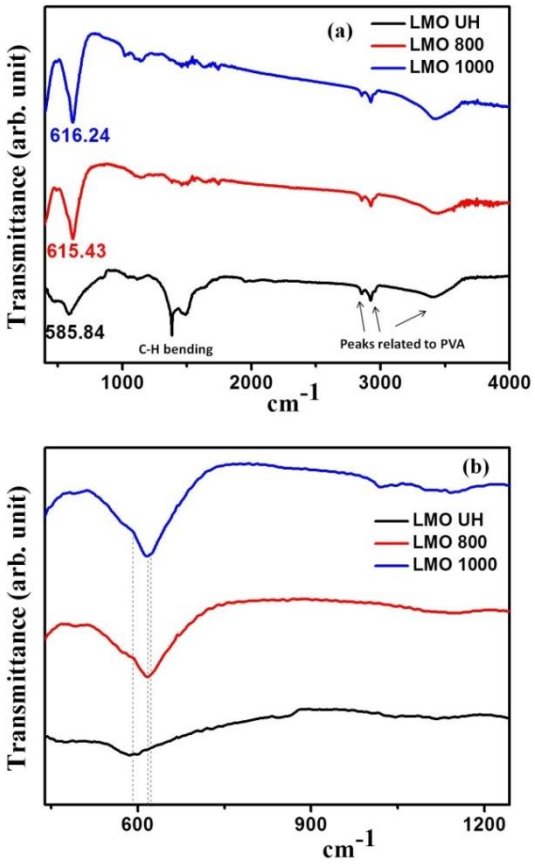

Fig. 3 – (a) FT-IR of LMO-UH, LMO-800 and LMO-1000 sample. (b) Enlarge FT-IR data for LMO-UH, LMO-800 and LMO-1000

material [31], which is in concurrence with our XRD result [Fig. 2(a)]. Moreover, the intensity found for this vibration band increases when the sample is calcined at 800 °C and 1000 °C, suggesting that the vibration bands become strong and up-shifting. Interestingly, we observed an apparent splitting of the M-O bond for LMO-800 and LMO-1000 [see dotted lines in Fig. 3 (b)], which was not observed for LMO-UH sample. This can be interpreted as a structural doublet that is allowed by the non-centrosymmetric MnO_6 octahedric groups [32, 33]. Such symmetry of MnO_6 group may be correlated to manganese ions that are in mixed valence states i.e., Mn^{3+} and Mn^{4+}. This could be resulting from the Jahn-Teller effects, which is partly related to the average ionic radius of the A sites and / or the oxygen deficiency. Moreover, it can also be based on the association with a supplementary polarization (dipole moment) of Mn-O bonds. With the calcinations, the changes in the LMO compound produce the shifting of M-O to higher frequencies determined by a decrease of symmetry of the lattice. This is the effect of the increase of the crystallites concentration per volume unit and the decrease of the MnO_6 groups symmetry i.e., in agreement with the XRD data [see Fig. 2 (a) and (b)]. Apart from this there are several other vibration bands found around ~ 1100 cm^{-1}, 3000 cm^{-1}, 3500 cm^{-1}, which appeared due to the impurity phases viz., C-H bending and / or originating from the consumed fuel i.e., PVA during the formation of the La-Mn-O perovskite material [34].

Fig. 4 illustrates the EDXRF spectra of a typical LMO-UH sample, while the compositional data for all the LMO samples are given in Table 1. It was seen from Table 1 that the chemical reactivity of the $LaMnO_3$ sample, especially, 'Mn-contents' goes on increasing when it is calcined by showing the increased concentration of the 'Mn'. The increase in the 'Mn' contents with calcinations indicates that probably, several Mn^{3+} ions starts getting converted into Mn^{4+}. Moreover, the increase in concentration of 'Mn' is seen to be compensated by the decrease in 'La' concentration. (Note that the other peak depicted in the EDXRF spectra originates from the sample holder). However, it is necessary to see the oxygen concentration and the effect of calcinations on it. Significantly, the ONH analysis (Table 1) indicated a decrease in oxygen contents with calcinations. When the sample is heated at 800 °C the environmental moisture loses, hence oxygen is removed from the surface of the material. Further heat treatment (i.e., LMO-1000 sample) causes the overheating, so that the sample starts to decompose. The decomposition of the crystal occurs with some sort of increased oxygen species. This explains that with heat treatment the compound becomes off-stiochiometric with respect to 'La' and 'O' resulting in more 'Mn' contents (with possible change in the charge state from Mn^{3+} to Mn^{4+} for charge balance).

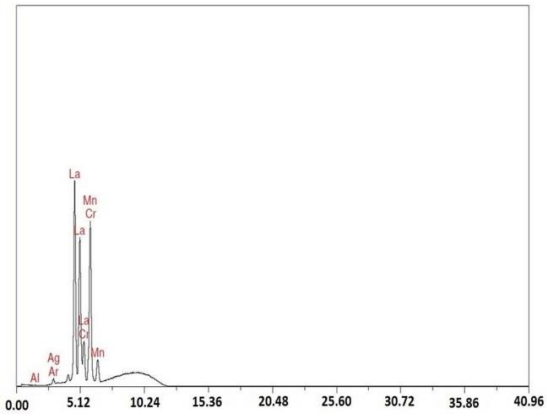

Fig. 4 – Typical EDXRF spectra of LMO-UH

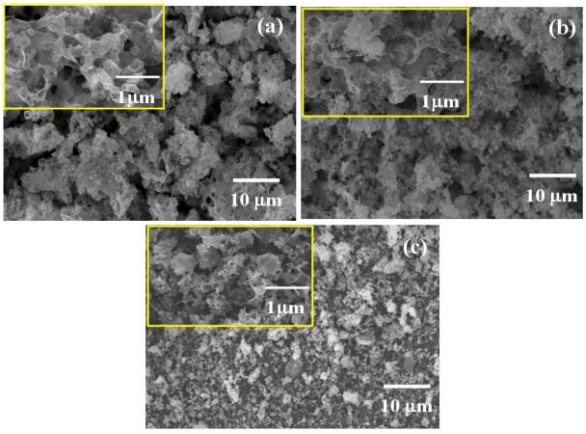

Fig. 5 – (a) SEM micrographs of LMO UH (10 μm × 2000) inset shows magnified image (1 μm × 20000) (b) SEM micrographs of LMO-800 (10 μm × 2000) inset shows magnified image (1 μm × 20000) (c) SEM micrographs of LMO-1000 (10 μm × 2000) inset shows magnified image (1 μm × 20000)

Morphological evaluation of the $LaMnO_3$ perovskite oxide is shown in Fig. 5 [(a)-(c)] for LMO-UH, LMO-800 and LMO-1000, respectively. Also shown in the inset of each respective figure is the higher resolution SEM image. The large area image indicates a spongy porous microstructure of the samples. Importantly, these spongy porous microstructures are agglomerated for LMO-UH sample, which with calcination reduces and gets separated. At higher resolutions, it was seen that the spongy porous microstructures looks more or less like a well defined porous foam-like structure for all the samples. Moreover, it was seen that with calcinations, the microstructure becomes more and more compact. Significantly, LMO-1000 samples show proper crystallization of the sample in the SEM image.

Table 1 – EDXRF and ONH analysis of LMO-UH, LMO-800 and LMO-1000 samples

	EDXRF		ONH Analysis		
Sample ID	Lanthanum (%)	Manganese (%)	Oxygen (%)	Nitrogen (%)	Hydrogen (%)
LMO UH	61.00 %	39.00 %	32.48 %	12.00 %	0.80 %
LMO 800	60.90 %	39.10 %	24.38 %	0.50 %	0.15 %
LMO 1000	60.00 %	40.00 %	25.00 %	9.35 %	0.30 %

Magnetic properties of the $LaMnO_3$ compound have been strongly correlated with the calcination tempera-

ture. Hysteresis (M-H) curve obtained at 30 K and 300 K for all the bulk $LaMnO_3$ samples i.e., LMO-UH, LMO-800 and LMO-1000 sample are shown in Fig. 6 [(a)-(c)], respectively. For sample LMO-UH, magnetization arises due to the impurities such as Mn_3O_4 present at the interstitial sites. The coercivity found at 30 K for this sample is around 710 Oe. Moreover, it is seen that the sample at larger applied fields shows a small increment in magnetization values. This may be again due to the presence of small impurity material, which opposes the spin alignment under the application of the external magnetic field. Saturation state as well as coercivity values were found to be changed when $LaMnO_3$ sample was calcined at 800 °C and 1000 °C. For LMO-800 and LMO-1000 the coercivity found at 30 K was around 54 Oe and 15 Oe, respectively, which is as shown in Fig. 6 (d). It indicate that the material resist largely to the magnetization when it is calcined at 800 °C and 1000 °C due to the increased crystalline size, tilts found in the MnO_6 octahedra and a more compactness of the microstructure [35]. Furthermore, the hysteresis loops obtained at room temperature shows paramagnetic behaviour.

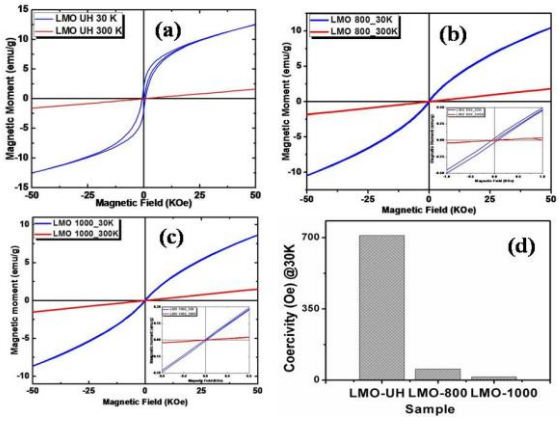

Fig. 6 (a) M-H curves of LMO UH taken at 30 K and 300 K (b) M-H curves of LMO-800 taken at 30 K and 300 K (c) M-H curves of LMO-1000 taken at 30 K and 300 K (d). Plot depicting the coercivity for LMO UH, LMO-800 and LMO-1000

The temperature dependent magnetization (M-T) obtained at Zero Field Cooling (ZFC) and Field Cooling (FC) by applying 0.5 KOe for the LMO-UH, LMO-800 and LMO-1000 samples are shown in Fig. 7 (a)-(c), respectively. It showed the considerable change in LMO-UH sample [Fig. 7 (a)] by dropping the magnetization with increase in temperature indicating a transition from ferromagnetic to the paramagnetic phase. Two transitions occurred around 100 K and 230 K with sharp decrease in magnetization for LMO-UH sample indicating the major role of the impurities in the sample [36]. In case of the LMO-800 [Fig. 7 (b)] and LMO-1000 [Fig. 7 (c)] sample, the M-T curves showed a sharp decrease in the magnetization in FC curves. At about 87 K, 47 K and 30 K, there is a peak in the ZFC curve of LMO-UH, LMO-800 and LMO-1000 samples, which corresponds to the blocking temperature T_b [37]. Moreover, it is seen in the ZFC curves of all the samples that there exhibits an increase in the magnetization as the temperature increases. After showing a maximum, the magnetization sharply decreases, which may be attributed to the coexistence of antiferromagnetic and ferromagnetic phases [38]. It is interesting to compare all these samples according to the evolution of magnetization due to the different response to the temperature. The main evolution attributes to the reduction in magnetization values, changes in the M-T curves with the calcinations of LMO sample, which attributes to consequent weakening in magnetic interaction [39]. This might be also in part due to an under-estimate of randomly distributed spins in LMO-800 and LMO-1000 sample. Since the spins are not well aligned after magnetizing the sample, suggests that there is a possibility of existence of superparamagnetism at low temperature in the sample. However, on the other hand spins on the Mn site are aligned properly in case of LMO-UH due to the application of the external magnetic field and also due to the presence of the impurities in the sample. This finding constitutes the direct evidence on how macroscopic properties can be controlled by calcining the LMO samples at different temperatures and hence manipulating the changes in the magnetic properties [40].

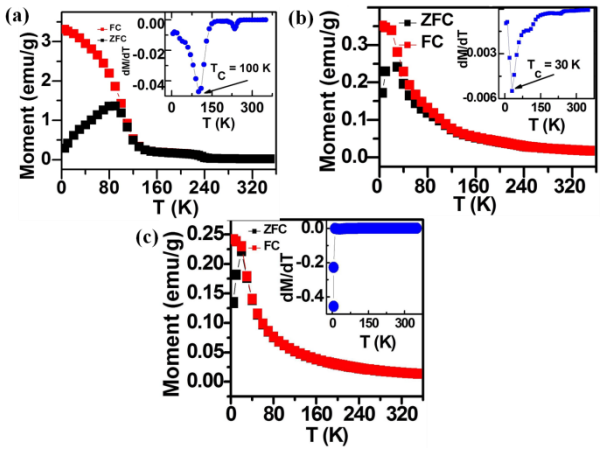

Fig. 7 – (a) M-T curve of LMO UH taken for zero field cooled (ZFC) and field cooled (FC) at 500 Oe (b) M-T curve of LMO-800 taken for zero field cooled (ZFC) and field cooled (FC) at 500 Oe (c) M-T curve of LMO-1000 taken for zero field cooled (ZFC) and field cooled (FC) at 500 Oe. (Inset of all figure shows the dM / dT vs temperature curve)

4. CONCLUSION

In conclusion, the structural as well as physical properties of the $LaMnO_3$ have been strongly influenced by the temperature; since the crystallinity and the crystalline size is controlled by the calcination temperature. The formation of superparamagnetic phase of orthorhombic $LaMnO_3$ at 800 °C is probably the result of weakly coupled spins. This indicates that the electron lattice interaction is sufficiently small La^{3+} cations, which manifest the global distortion in the perovskite structure that depends on the degree of tilting of MnO_6 octahedron. The progressive degree of an average tilting of MnO_6 octahedron controls the transition temperature of the $LaMnO_3$. Moreover, the temperature effect on the $LaMnO_3$ matrix probably increases the Mn oxidation state; therefore, it gives the unusual dependence of the magnetization with temperature.

AKNOWLEDGEMENTS

One of the authors NGD has express gratitude to Department of Science and Technology (DST), Govt. of India, for awarding DST-INSPIRE Faculty award. ARS is also thankful to DST INSPIRE faculty award research project for project assistanceship. We are thankful to Centre of Inter Disiplinary, Dr. D.Y. Patil University, Kolhapur for making a fruitful discussion. We are also thankful to Mr. M.S. Seo, KBSI, Daejon, Korea for providing magnetic measurement.

REFERENCES

1. P. Ravindran, A. Kjekshus, H. Fjellvag, A. Delin, O. Eriksson, *Phys. Rev. B* **65**, 064445 (2002).
2. M.V. Abrashev, A.P. Litvinchuk, M.N. Iliev, R.L. Meng, V.N. Popov, V.G. Ivanov, R.A. Chakalov, C. Thomsen, *Phys. Rev. B* **59**, 4146 (1999).
3. T. Grande, J.R. Tolchard, S.M. Selbach, *Chem. Mater.* **24**, 338 (2012).
4. P. Mondal, D. Bhattacharya, P. Mandal, *Phys. Rev. B* **84**, 075111 (2011).
5. V. Markovich, G. Jung, I. Fita, D. Mogilyansky, X. Wu, A. Wisniewski, R. Puzniak, N. Froumin, L. Titelman, L. Vradman, M. Herskowitz, G. Gorodetsky, *J. Phys. D: Appl. Phys.* **41**, 185001 (2008).
6. R.A. De Souza, M.S. Islamb, E.I. Tiffee, *J. Mater. Chem.* **9**, 1621 (1999).
7. K. Rosciszewski, A.M. Ole, *J. Phys.: Condens. Matter.* **22**, 425601 (2010).
8. P.R. Huang, Y. He, C. Cao, Z.H. Lu, *Sci. Rep.* **4**, 7131 (2014).
9. N.G. Deshpande, C.H. Weng, Y.F. Wang, Y.C. Shao, C.Q. Cheng, D.C. Ling, H.C. Hsueh, C.H. Du, H.M. Tsai, C.W. Pao, H.J. Lin, J.F. Lee, J.W. Chiou, M.H. Tsai, W.F. Pong, *J. Appl. Phys.* **115**, 233713 (2014).
10. P. Schlottmann, *J. Appl. Phys.* **103**, 07F717 (2008).
11. A. Nucara, A. Perucchi, P. Calvani, T. Aselage, D. Emin, *Phys. Rev. B* **68**, 174432 (2003).
12. H. Khanduri, M.C. Dimri, S. Vasala, S. Leinberg, R. Lohmus, T.V. Ashworth, A. Mere, J. Krustok, M. Karppinen, R. Stern, *J. Phys. D: Appl. Phys.* **46**, 175003 (2013).
13. M.V. Kuznetsov, I.P. Parkin, D.J. Caruanab, Y.G. Morozov, *J. Mater. Chem.* **14**, 1377 (2004).
14. R. Suryanarayanana, J. Berthon, I. Zelenay, B. Martinez, X. Obradors, S. Uma, E. Gmelin, *J. Appl. Phys.* **83**, 5264 (1998).
15. T. Chatterji, F. Fauth, B. Ouladdiaf, P. Mandal, B. Ghosh, *Phys. Rev. B* **68**, 052406 (2003).
16. X. Zhou, J. Xue, D. Zhou, Z. Wang, Y. Bai, X. Wu, X. Liu, J. Meng, *ACS Appl. Mater. Interf.* **2**, 2689 (2010).
17. M. Salluzzo, S. Gariglio, D. Stornaiuolo, V. Sessi, S. Rusponi, C. Piamonteze, G.M. De Luca, M. Minola, D. Marre, A. Gadaleta, H. Brune, F. Nolting, N.B. Brookes, G. Ghiringhelli, *Phys. Rev. Lett.* **111**, 087204 (2013).
18. C. He, T.D. Sanders, M.T. Gray, F.J. Wong, V.V. Mehta, Y. Suzuki, *Phys. Rev. B* **86**, 081401 (2012).
19. X.L. Wang, D. Li, C.X. Shi, B. Li, T.Y. Cui, Z.D. Zhang, *Physica B* **405**, 1362 (2010).
20. M.V. Abrashev, A.P. Litvinchuk, M.N. Iliev, R.L. Meng, V.N. Popov, V.G. Ivanov, R.A. Chakalov, C. Thomsen, *Phys. Rev. B* **59**, 4146 (1999).
21. P. Orgiani, A. Galdi, C. Aruta, V. Cataudella, G. De Filippis, C.A. Perroni, V.M. Ramaglia, R. Ciancio, N.B. Brookes, M.M. Sala, G. Ghiringhelli, L. Maritato, *Phys. Rev. B* **82**, 205122 (2010).
22. W.J. Lu, Y.P. Sun, B.C. Zhao, X.B. Zhu, W.H. Song, *Phys. Rev. B* **73**, 174425 (2006).
23. U.D. Wdowik, B. Ouladdiaf, T. Chatterji, *J. Phys.: Condens. Matter.* **23**, 245402 (2011).
24. W.J. Lu, Y.P. Sun, B.C. Zhao, X.B. Zhu, W.H. Song, *Phys. Rev. B* **73**, 174425 (2006).
25. P. Murugavel, J.H. Lee, Y.G. Yoon, T.W. Noh, J.S. Chung, M. Heu, S. Yoon, *Appl. Phys. Lett.* **82**, 1908 (2003).
26. W.S. Choi, Z. Marton, S.Y. Jang, S.J. Moon, B.C. Jeon, J.H. Shin, S.S.A. Seo, T.W. Noh, K. Myung-Whun, H.N. Lee, Y.S. Lee, *J. Phys. D: Appl. Phys.* **42**, 165401 (2009).
27. R. Zhao, K. Jin, Z. Xu, H. Guo, L. Wang, *Appl. Phys. Lett.* **102**, 122402 (2013).
28. P. Barpanda, N. Recham, J.N. Chotard, K. Djellab, W. Walker, M. Armanda, J.M. Tarascon, *J. Mater. Chem.* **20**, 1659 (2010).
29. H. Wanga, Z. Zhaoa, C.M. Xua, J. Liu, *Cata. Lett.* **102**, 251 (2005).
30. M.V. Kuznetsov, I.P. Parkin, D.J. Caruanab, Y.G. Morozov, *J. Mater. Chem.* **14**, 1377 (2004).
31. J.J.U. Buch, G. Lalitha, T.K.P. Athak, N.H.V. Asoya, V.K. Lakhani, *J. Phys. D: Appl. Phys.* **41**, 025406 (2008).
32. P. Mondal, D. Bhattacharya, P. Choudhury, P. Mandal, *Phys. Rev. B* **76**, 172403 (2007).
33. C.S. Nelson, J.P. Hill, D. Gibbs, F. Yakhou, F. Livet, Y. Tomioka, T. Kimura, Y. Tokura, *Phys. Rev. B* **66**, 134412 (2002).
34. E.S. Toberer, J.C. Weaver, K. Ramesha, R. Seshadri, *Chem. Mater.* **16**, 2194 (2004).
35. B. Ghosh, V. Siruguri, A.K. Raychaudhuri, T. Chatterji, *J. Phys.: Condens. Matter.* **26**, 025603 (2014).
36. S. Salem-Sugui Jr., A.D. Alvarenga, R.D. Noce, R.B. Guimarães, C. Salazar Mejia, H. Salim, F.G. Gandra, *AIP Adv.* **2**, 032168 (2012).
37. V. Markovich, G. Jung, I. Fita, D. Mogilyansky, X. Wu, A. Wisniewski, R. Puzniak, N. Froumin, L. Titelman, L. Vradman, M. Herskowitz, G. Gorodetsky, *J. Phys. D: Appl. Phys.* **41**, 185001 (2008).
38. T.I. Arbuzova, B.A. Gizhevskii, R.G. Zakharov, S.A. Petrova, N.M. Chebotaev, *Phys. Solid State* **50**, 1487 (2008).
39. L. Ghivelder, I.A. Castillo, M.A. Gusmao, J.A. Alonso, L.F. Cohen, *Phys. Rev. B* **60**, 12184 (1999).
40. W.J. Lu, Y.P. Sun, B.C. Zhao, X.B. Zhu, W.H. Song, *Phys. Rev. B* **73**, 174425 (2006).